

# Pulsed diode laser-based singlet oxygen monitor for photodynamic therapy: *in vivo* studies of tumor-laden rats

Seonkyung Lee  
Danthu H. Vu  
Michael F. Hinds  
Steven J. Davis

Physical Sciences Inc.  
20 New England Business Center  
Andover, Massachusetts 01810-1077  
E-mail: lee@psicorp.com

Alvin Liang  
Tayyaba Hasan

Massachusetts General Hospital  
Wellman Laboratories of Photomedicine  
40 Blossom Street  
Boston, Massachusetts 02114-2605

**Abstract.** Photodynamic therapy (PDT) is a promising cancer treatment that involves optical excitation of photosensitizers that promote oxygen molecules to the metastable  $O_2(a^1\Delta)$  state (singlet oxygen). This species is believed to be responsible for the destruction of cancerous cells during PDT. We describe a fiber optic-coupled, pulsed diode laser-based diagnostic for singlet oxygen. We use both temporal and spectral filtering to enhance the detection of the weak  $O_2(a \rightarrow X)$  emission near  $1.27 \mu\text{m}$ . We present data that demonstrate real-time singlet oxygen production in tumor-laden rats with chlorin e6 and 5-aminolevulinic acid-induced protoporphyrin photosensitizers. We also observe a positive correlation between post-PDT treatment regression of the tumors and the relative amount of singlet oxygen measured. These results are promising for the development of the sensor as a real-time dosimeter for PDT. © 2008 Society of Photo-Optical Instrumentation Engineers. [DOI: 10.1117/1.3042265]

Keywords: photodynamic therapy; singlet oxygen; light dosimetry.

Paper 08227R received Jul. 11, 2008; revised manuscript received Oct. 24, 2008; accepted for publication Oct. 25, 2008; published online Dec. 18, 2008; corrected Dec. 29, 2008.

## 1 Introduction

Photodynamic therapy (PDT) is an emerging cancer treatment that uses photosensitizers activated with visible wavelength light. The photoactivated photosensitizer (PS) excites oxygen to the ( $a^1\Delta$ ) state via the type-II photochemical pathway.<sup>1</sup> Previous studies have provided strong evidence that singlet oxygen is the active species in cancer cell or endothelial cell necrosis.<sup>2-6</sup> Thus, a device that facilitates the measurement of the singlet oxygen *in vivo* could provide a crucial parameter in PDT dosimetry and the potential of improved and even individualized therapeutic design.

There has been considerable interest in developing a sensor for singlet oxygen that could be used as a real-time dosimeter during PDT treatments.<sup>7-19</sup> Correlations of the singlet oxygen produced with treatment efficacy could be one important use of such a sensor. Some researchers have attempted to develop dosimeters based on the prompt, radiatively allowed fluorescence of the PS in the tumor, but simple PS fluorescence detection may not accurately reflect the complex and dynamic interactions that lead to the therapeutic effect.<sup>3</sup> Pogue et al.<sup>11</sup> used small electrodes to measure total oxygen content in tumors during PDT in animal studies and demonstrated deoxygenation during treatments. Other researchers have shown that oxygenation of tissue can enhance PDT efficiency.<sup>12-14</sup>

Some of the earlier work used sensitive but slow (bandwidths on the order of  $10^{-3}$  s) detectors for the  $1.27\text{-}\mu\text{m}$  sin-

glet oxygen emission. While these proved useful for *in vitro* studies, this approach was unsuccessful *in vivo* due to the slow detector response. Recently, a high quantum efficiency, high speed ( $\sim 7$  ns), low dark current photomultiplier tube (PMT) became commercially available, and this greatly enhanced detection of the weak singlet oxygen emission near  $1.27 \mu\text{m}$ . Using this detection method, we have developed a sensitive, diode laser-based monitor for singlet oxygen produced by PDT.<sup>15-17</sup> In Fig. 1, we illustrate our detection strategy that includes both temporal discrimination and spectral filtering to maximize the sensitivity of our system to singlet oxygen emission. The pioneering work of Wilson, Patterson, and Lilge<sup>8</sup> has also described a singlet oxygen monitor based on similar detection methods. However, there are significant differences between the two approaches. Wilson's group used a Q-switched, frequency-doubled, Nd:YAG laser (pulse lengths  $\sim 10$  ns) in contrast to our relatively long ( $\sim 1$  to  $10 \mu\text{s}$ ) pulses. Diode laser pulses do not produce significant energy compression, and the peak power of the diode laser ( $< 300$  mW) is much less than that of Q-switched devices. In addition, our system is fiber coupled; the diode laser beam delivery and the singlet oxygen collection are both facilitated by fiber optic cables, where Wilson, Patterson, and Lilge used free-space optics. More recently, Maisch et al.<sup>18</sup> used a Q-switched Nd:YAG laser and the PMT approach to detect singlet oxygen produced by PDT in bacteria. Yamamoto et al.<sup>19</sup> have used a Q-switched Nd:YAG laser-pumped dye laser to produce and monitor singlet oxygen both *in vitro* and *in vivo*.

Address all correspondence to: Seonkyung Lee, Physical Sciences Inc., 20 New England Business Center, Andover, MA 01810; Tel: 978-689-0003; Fax: 978-689-3232; E-mail: lee@psicorp.com

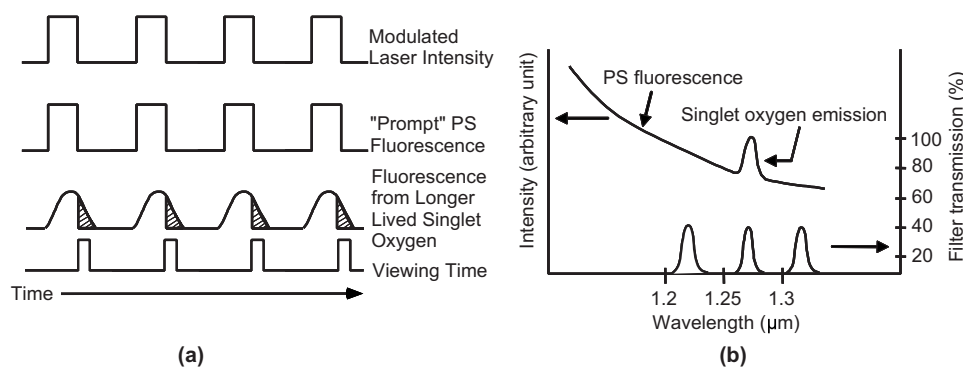


**Fig. 1** Detection scheme for singlet oxygen emission with a short pulse diode laser: (a) temporal filtering method using pulsed diode laser, and (b) typical spectra for photosensitizer fluorescence, singlet oxygen emission, and the transmission curves of the three filters used to isolate the singlet oxygen emission.

Previously, we described an early version of our singlet oxygen monitor and demonstrated that we could measure the production of singlet oxygen in a variety of singlet oxygen quenching media including water, methanol, acetone, and protein-rich aqueous solutions.<sup>15–17</sup> Here we report the detection of singlet oxygen on tumor-laden rats with the photosensitizers chlorin e6 (*Cl-e6*) and 5-aminolevulinic acid-induced protoporphyrin (ALA-induced Pp IX). We observed a positive correlation between the observed singlet oxygen signal and the post-treatment regression of tumors on several rats.

## 2 Method

### 2.1 Apparatus and Measurement of Singlet Oxygen

We used time-resolved emission measurements and optical filtering to enhance the sensitivity for detecting the singlet oxygen, as shown in Fig. 1. The temporal filtering method is outlined in Fig. 1(a), and the spectral filtering to further isolate the singlet oxygen emission (near  $1.27 \mu\text{m}$ ) from long wavelength PS fluorescence and/or phosphorescence is shown in Fig. 1(b). It is well established that singlet oxygen is severely quenched in aqueous media. Indeed, the lifetime is reduced from about 60 min in the gas phase to approximately  $4 \mu\text{s}$  in aqueous media. In biological media, however, the lifetime is further reduced to around 100 ns.<sup>13,14</sup> This is one of the major challenges of detecting singlet oxygen both *in vitro* and *in vivo*. The high bandwidth, near infrared (IR) PMT and a temporally gated detection system help isolate the longer lived singlet oxygen emission from the much faster PS fluorescence. Two diode lasers were used in the singlet oxygen sensor: 1. 655-nm, 5- $\mu\text{s}$  pulse width, 1-kHz repetition rate for *Cl-e6*, and 2. 635-nm, 5- $\mu\text{s}$  pulse width, 10-kHz repetition rate for ALA.

The singlet oxygen detection system includes: 1. the diode laser module; 2. optical filters/PMT detection system; and 3. the data acquisition system with a photon counting board. Both the pulsed diode laser light delivery and singlet oxygen emission collection are fiber optic-coupled via a bifurcated probe, and this facilitates application of the sensor to *in vivo* studies. The excitation light was delivered to the site being examined by one leg of the fiber optic, and the near-IR emission was collected by the other leg. The detected emission included the singlet oxygen signal and other possible near-IR

radiation such as PS fluorescence, phosphorescence, and tissue autofluorescence. At the distal end of the detection fiber, the near-IR radiation was collimated and sent through a series of three narrow bandpass filters (15-nm bandwidths and transmission center wavelengths of 1.22, 1.27, and  $1.315 \mu\text{m}$ ) contained in a sliding filter holder configuration. At each bandpass filter wavelength, the signal was accumulated over 30,000 laser pulses, typically 3 sec with 10-kHz operation. The filters provided spectral discrimination of the singlet oxygen emission from the interferences mentioned before. The emission feature of singlet oxygen is centered in the wavelength region of  $1.27 \mu\text{m} \pm 10 \text{ nm}$ . The two filters centered at 1.22 and  $1.315 \mu\text{m}$  provided measurements of the background emission that did not contain singlet oxygen emission. The optical radiation transmitted by the filters was detected by a thermoelectrically cooled PMT (Hamamatsu model H9170-45, NJ, USA) run in a photon counting mode. The output current pulses from the PMT were amplified with a high bandwidth amplifier and fed to the data acquisition system. We combined the acquisition system with a fast photon counting board (Becker and Hickl model MSA-300, MA, USA) that can handle up to a 20-kHz operation rate for our system configuration.

For our initial *in vivo* measurements with *Cl-e6*, we used only one filter centered at a wavelength of  $1.27 \mu\text{m}$ . The background signal subtraction was done with a signal measured at an off-tumor site distinct from the tumor site. The off-tumor site retains much less PS, so the detected signal is predominantly due to scattered light from the irradiated tissue. However, we found large variations of background signal due to differing skin optical characteristics at different locations within the same animal. With only one optical filter at  $1.27 \mu\text{m}$ , these variations severely affected the background subtraction method used to extract the singlet oxygen emission signal, especially for weaker singlet oxygen signals. Thus, to minimize signal variations due to skin optical characteristics and to enhance the detection sensitivity, we introduced the three filter method. This allowed measurement of both the singlet oxygen and background emissions over the same area of skin.

Our system produces the detected singlet oxygen emission by the type-II process. The pulsed diode laser in our sensor is distinct from the cw PDT treatment laser. The pulsed diode

laser produces singlet oxygen from ground state oxygen within the tissue that is available at various times before, during, and after the treatments by the cw PDT laser. The singlet oxygen that we measure is proportional to the product of the available ground state oxygen concentration multiplied by the PS concentration (i.e.,  $[^1\text{O}_2] \propto [\text{PS}] \times [\text{O}_2]$ ). In our system, this measurement is done at various times before and during the PDT treatments. The cw treatment laser is shut off for a short period ( $\sim 30$  s), and the pulsed diode laser is used to produce singlet oxygen. Thus, our monitor measures the capacity of the irradiated tissue to produce singlet oxygen, and the measured signal is assumed to be proportional to the singlet oxygen produced when the PDT treatment laser is on. In future work, we plan to pulse the treatment laser to provide singlet oxygen emission signals directly during PDT treatment.

## 2.2 Protocol for Animal Study

We measured singlet oxygen production in tumor-laden rats during PDT treatment using the singlet oxygen monitor at the Wellman Laboratories of Photomedicine at Massachusetts General Hospital (MGH). The animal model used the R3327-MatLyLu prostate cancer cell line that somewhat follows the human disease pattern and metastasizes into lymph nodes and lungs. Since the R3327-MatLyLu cells are syngeneic, there is no need for immune suppression in the rats, which enhances the model's clinical relevance. This study was performed under MGH protocol and was reviewed and approved by the MGH Subcommittee on Research Animal Care (SRAC)-OLW Assurance (title of protocol: Measurement of Singlet Oxygen Formation During Photodynamic Therapy Using a Diode Laser-Based System: Rats Model).

Tumors were induced by subcutaneous injection of a suspension of  $10^5$  R3327-MatLyLu cells into the flanks of two-month-old male Copenhagen rats of 150- to 200-g weight. Once the tumors had reached treatment size, the animals received an injection of either intravenous *Cl-e6* or intraperitoneal ALA. After a waiting period of 3 h that allows for accumulation of PS in the tumor, light exposure was done in the anesthetized animals through the shaved skin.<sup>20,21</sup> Treatment irradiations of the tumors were performed using cw diode laser sources (HPD, Incorporated) with a wavelength that matched the absorption profile of the PS; 655-nm diode laser for *Cl-e6*, and 635-nm diode laser for ALA. The incident power density of the treatment laser was  $100 \text{ mW/cm}^2$ .

The singlet oxygen probe was placed 1.5 mm above the skin of the subject animals. The singlet oxygen emissions were recorded at several times: 1. before infusion of a PS, 2. immediately before starting the therapeutic light exposure but after the PS had spread systemically for a specific PS incubation time period, 3. at several separate times during the therapeutic irradiation, and 4. at the end of the light exposure. Each measurement contained 30,000 pulses from the diode laser source. The measurement required interrupting the therapeutic light exposure, but only for approximately 10 to 30 s. Using the singlet oxygen monitor in this way does not influence PDT treatment protocols.

We recorded tumor growth after PDT treatment with a control group and different ALA dosage groups: 100 and 200 mg/kg body weight of ALA, and 50 and 25 J/cm<sup>2</sup> of

total light dosage. For the tumor regression study, implant sizes were repeatedly assessed by caliper measurement. Tumor volumes ( $V$ ) were calculated using the formula for the ellipsoid  $V = \text{length} \times \text{width} \times \text{height} \times 0.5236$  ( $\pi/6$ ). Tumors were observed while growing to treatment dimensions of about  $0.3 \text{ cm}^3$ , which requires approximately 8 to 10 days. The animals were sacrificed at 14 days from the day of PDT treatment.

## 3 Results and Discussion

### 3.1 Kinetic Model for Singlet Oxygen

We interpret the observed signals of the singlet oxygen emission using a kinetic model described earlier<sup>17</sup> and summarized next. Assuming that the singlet oxygen is produced via the type-II mechanism and treating the excitation pulse as an “instantaneous” source, leads to a time-dependent solution for the singlet oxygen concentration  $[\text{O}_2(^1\Delta)]_t$  in  $\text{cm}^{-3}$  after the termination of the excitation pulse, given by:

$$[\text{O}_2(^1\Delta)]_t = N\sigma[S_o]\Phi_{\Delta} \frac{\tau_{\Delta}}{\tau_T - \tau_{\Delta}} \{ \exp(-t/\tau_T) - \exp(-t/\tau_{\Delta}) \}, \quad (1)$$

where  $N$  is the number of photons per  $\text{cm}^2$  in the excitation pulse incident on the sample,  $\sigma$  is the absorption cross section of the PS in  $\text{cm}^2$ ,  $[S_o]$  is the concentration of PS ground state,  $\Phi_{\Delta}$  is the quantum yield of singlet oxygen, and  $\tau_T$  and  $\tau_{\Delta}$  are lifetimes of PS triplet state and singlet oxygen, respectively.

This is identical to the result discussed in Refs. 8–10, where they used a Q-switched, frequency-doubled, Nd:YAG laser or an optical parametric oscillator as the excitation source. Both produce very short pulses ( $\sim 10$  ns), and Eq. (1) is an adequate description. However, our diode laser approach uses much longer pulses (1 to 10  $\mu\text{s}$ ), and the instantaneous excitation model is no longer valid while the diode laser is on. In our case, the diode laser intensity is constant over the duration of the pulse, and the kinetics of singlet oxygen production and destruction during the laser pulse become non-negligible. To gain a better understanding of this long pulse limit, we solved this kinetic model numerically using MathCAD. An example of this model study is shown in Fig. 2. During the diode laser pulse, the population of the PS singlet state quickly reaches a steady state value [Fig. 2(a)]. The PS triplet state population grows and populates the oxygen singlet state via energy transfer collisions during the laser pulse [Fig. 2(b)]. The total temporal profile [Fig. 2(c)] is the sum of the emissions from both the PS and the singlet oxygen. We readily observed these processes in several *in vitro* studies, as shown in Fig. 2(d).<sup>17</sup> Some data observed in the present *in vivo* studies also displayed both the growth of the singlet oxygen signal in the early part of the diode laser pulse and its decay subsequent to the laser pulse.

Figures 2(e) and 2(f) show comparisons of this model to our data from aqueous solutions with two different excitation pulse widths: 1 and 5  $\mu\text{s}$ . (Note that we collect data for 6  $\mu\text{s}$  prior to the initiation of the diode laser pulse to provide a “zero” level for the subsequent data reduction.) Many photosensitizers produce some prompt PS singlet state emission even at the singlet oxygen emission wavelength of 1.27  $\mu\text{m}$ .

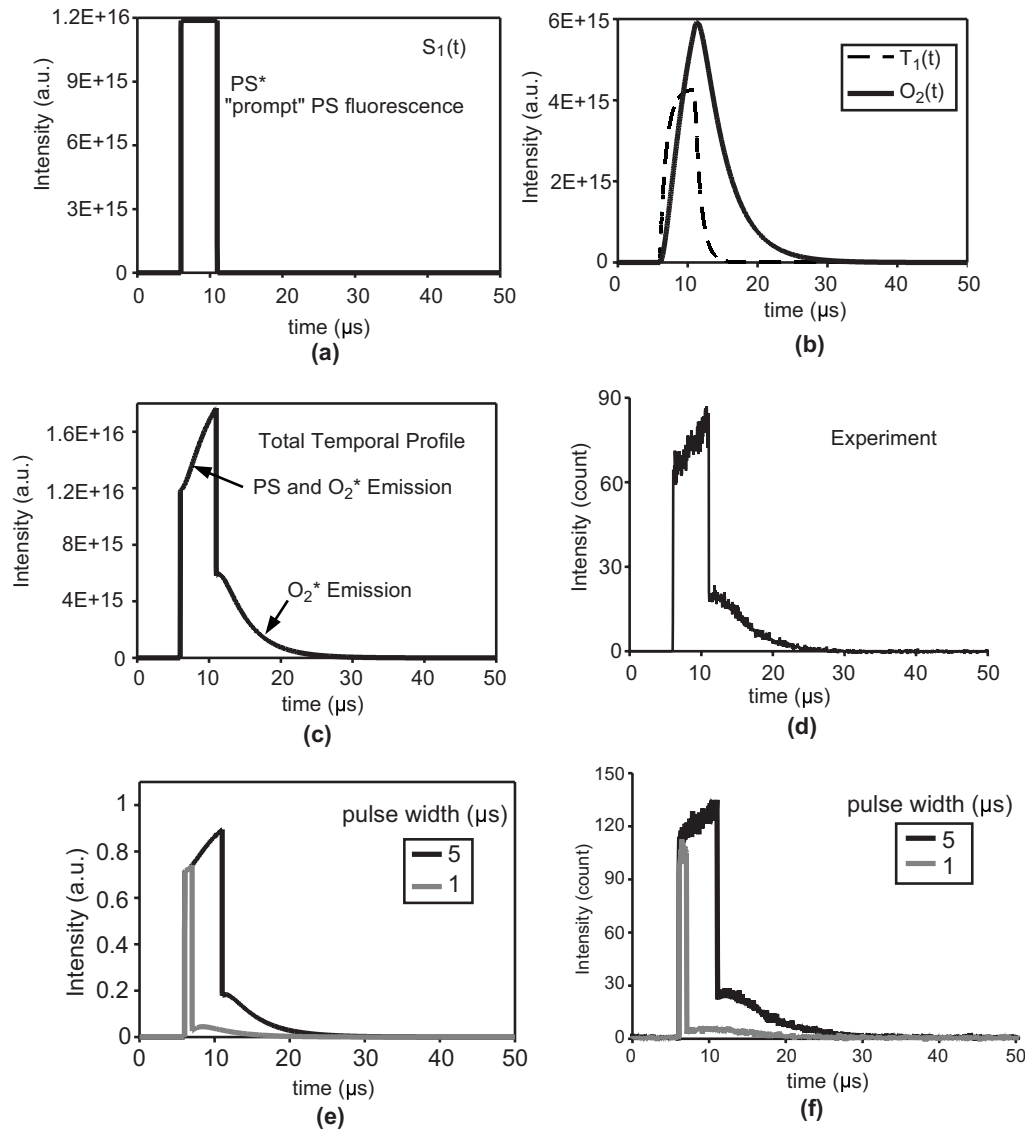


**Fig. 2** Kinetic model predictions compared to experimental emission profiles: (a), (b), and (c) model calculations showing components of the PDT process for long pulse (5  $\mu\text{s}$ ) diode laser excitation; and (d) data from *in vitro* measurements. Temporal profiles for the radiative emission from singlet oxygen in water with different laser pulse widths: (e) prediction using our kinetic model with  $\tau_T=1 \mu\text{s}$ ,  $\tau_\Delta=4 \mu\text{s}$ ,  $\Phi_T=0.4$ ,  $\Phi_\Delta=0.7$ ; and (f) experimental results with *Cl-e6* in aqueous solution.

This PS fluorescence decays in a few nanoseconds after the diode laser pulse is terminated, as shown in both our model and experimental measurements. Using PDT treatment parameters such as PS concentration, laser intensity, PS triplet lifetime, singlet oxygen lifetime, and energy transfer rates, the model provides a guide for the interpretation of the singlet oxygen production in the solution phase. The model also implies that there may be an optimum diode laser pulse width to maximize the singlet oxygen produced per pulse, and this may enable one to develop optimized conditions of PDT treatments.

### 3.2 Singlet Oxygen Detection in Tumor-Laden Rats

Our first experiments to investigate the detection sensitivity for singlet oxygen *in vivo* used *Cl-e6* and only the 1.27- $\mu\text{m}$  bandpass filter for spectral discrimination of the singlet oxygen emission. We recorded the temporal evolutions of the

emission at 1.27  $\mu\text{m}$  and integrated the emission signal counts over the time interval of 2 to 4  $\mu\text{s}$  after the termination of the diode laser pulse. The singlet oxygen and background signals were measured at two distinct locations on each rat. The background emission signals were recorded at a location that did not include tumor tissue. The singlet oxygen emission plus any background signals were measured on the tumor site. The signal of singlet oxygen produced from the tumor site was calculated by subtracting the background emission (off-tumor site) from the emission observed on the tumor site. This measurement (in photoelectron counts) provided a relative value for the singlet oxygen concentration produced by the pulsed diode laser. For the *in vivo* studies, we used two diode laser sources: a continuous wave (cw) treatment laser and a pulsed laser for the singlet oxygen measurements. We controlled the total PDT treatment light fluence of the cw

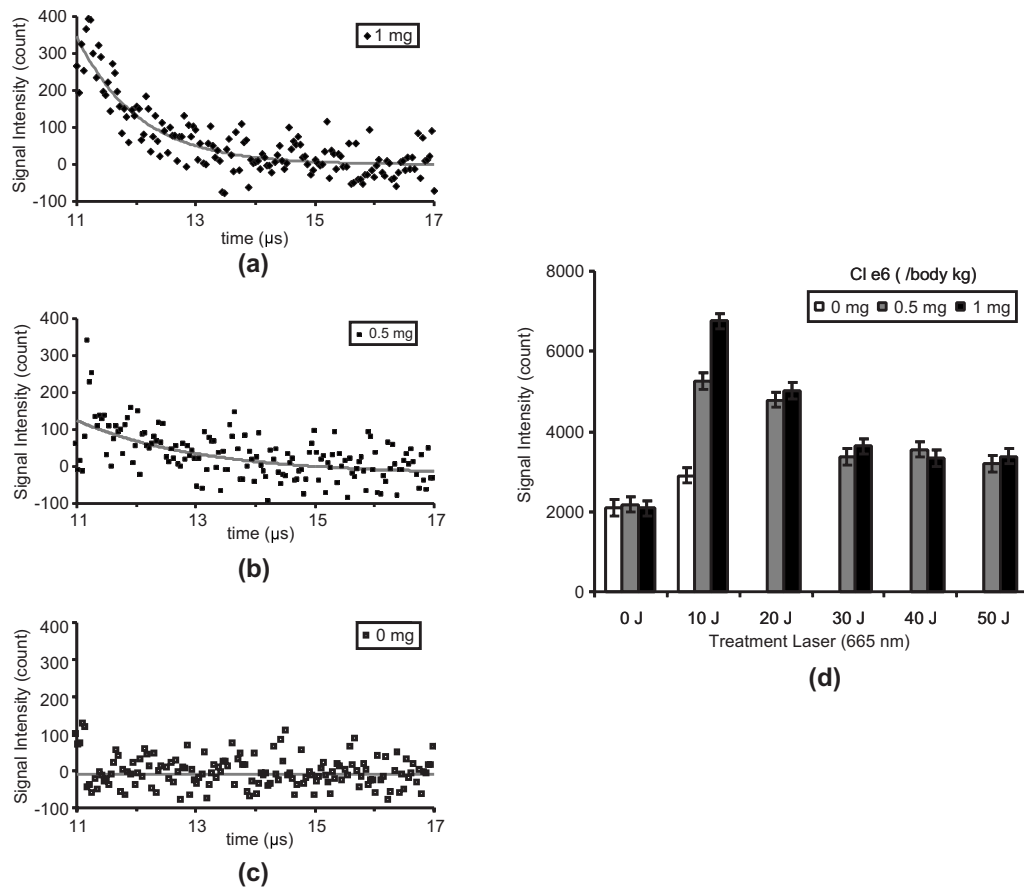


**Fig. 3** Singlet oxygen temporal profiles of emission signals from tumor-laden rats with several dosages of (a) 1 mg, (b) 0.5 mg, (c) 0 mg *Cl-e6*/kg body, and (d) singlet oxygen production in rats measured during PDT light treatment.

laser, and made the singlet oxygen measurements during short periods of time when the cw laser was off.

Figures 3(a)–3(c) show typical temporal profiles (background subtracted) in photoelectron counts at  $1.27 \mu\text{m}$  immediately after a  $10 \text{ J}/\text{cm}^2$  light treatment with a 655-nm diode laser for three tumor-laden rats. One had no *Cl-e6*, one was infused to a *Cl-e6* concentration of 0.5 mg/kg body weight, and the third was infused to a *Cl-e6* concentration of 1 mg/kg body weight. The data indicate a correlation between the temporal profiles of singlet oxygen emission and the initial concentrations of the infused *Cl-e6*. Figure 3(d) summarizes the observed singlet oxygen production with different PDT light irradiations for three tumor-laden rats with *Cl-e6*. These data represent the summation of photoelectron counts (after background subtraction) at  $1.27 \mu\text{m}$ . For these data, the singlet oxygen was measured at two locations on the tumor in each rat, and the data show the two-site average signal of the singlet oxygen production as a function of total PDT treatment light fluence. We observed photoelectrons that we interpret as being due to singlet oxygen emission in the control group that had no *Cl-e6*. This is most likely due to singlet oxygen production from naturally existing porphyrins in the skin, as reported by other groups.<sup>10</sup> After  $10 \text{ J}/\text{cm}^2$  of PDT treatment with the cw treatment laser, there was a distinct increase in the singlet oxygen signal. Subsequent to further treatment, the data show a reduction of the singlet oxygen

signal as the total light dose was increased. The causes of this diminution are likely a combination of tumor hypoxia and *Cl-e6* photobleaching.

While the background subtraction method was adequate for the *Cl-e6* photosensitizer that produced relatively large singlet oxygen emissions, other photosensitizers, e.g., ALA, produce considerably smaller singlet oxygen signals as we observed in previous *in vitro* studies.<sup>15–17</sup> Consequently, to enhance the sensitivity of the singlet oxygen monitor, we added two optical filters that pass near-IR radiation at 1.22 and  $1.315 \mu\text{m}$  (shorter and longer wavelengths than the singlet oxygen emission wavelength). All three filters were contained in a sliding filter holder to allow rapid and reproducible insertion of each filter into the optical detection path. The observed signals with the bandpass filters centered at 1.22 and  $1.315 \mu\text{m}$  were used to improve the background subtraction routine and provide more accurate determination of the singlet oxygen signal. The average value of the signals at 1.22 and  $1.315 \mu\text{m}$  was subtracted from the signal recorded with the  $1.27\text{-}\mu\text{m}$  bandpass filter to obtain the singlet oxygen signal. These measurements were made sequentially but at the same location on the rats. The background signals may contain photosensitizer fluorescence, phosphorescence, and autofluorescence of any of the optical components, including the collection fiber optics.

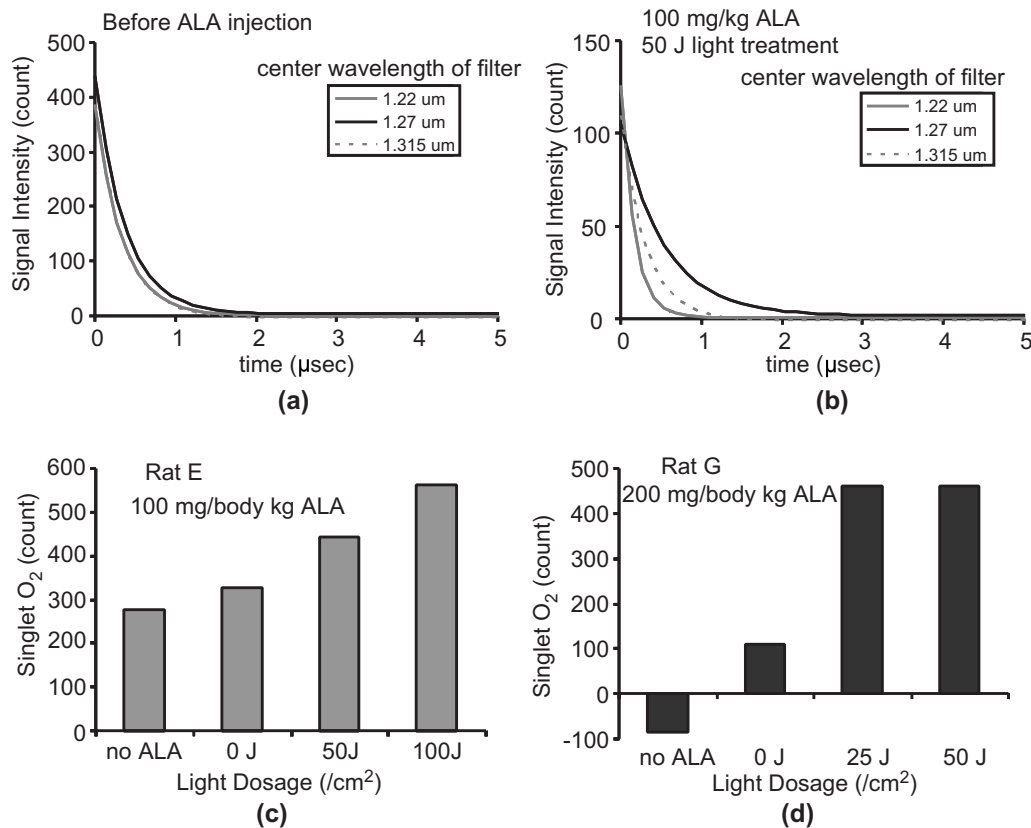


**Fig. 4** Typical decay profiles of singlet oxygen produced in a single tumor laden rat: (a) before ALA injection, and (b) after 100-mg/kg body ALA injection and PDT treatment with 50-J/ $\text{cm}^2$  irradiation from a 635-nm diode laser. Singlet oxygen produced (in photoelectron counts) from a tumor implanted on a rat as a function of total PDT light dosage (c) and (d). Data were collected with a 635-nm diode laser in prostate-tumor-laden rats.

In the ALA study, we used this three-filter detection method and a 635-nm diode laser for the PDT treatment light source. The singlet oxygen production was measured with a 635-nm pulsed diode laser 1. before ALA injection, 2. just before PDT treatment after 3 h of ALA incubation time period, 3. between the PDT treatment, and 4. at the end of the PDT treatment. The tumor size was recorded for 14 days following PDT treatment.

Figures 4(a) and 4(b) show fits to data for a single animal but are typical for the ALA study. Figure 4(a) shows the averages of 30,000 diode laser pulses prior to injection with ALA, each at the three wavelengths transmitted by the narrow bandpass filters. These data demonstrate that optical signals are observed at all three wavelengths, probably due to broadband PS fluorescence and phosphorescence. Since we extract the singlet oxygen signal using the difference between the signal at 1.27  $\mu\text{m}$  and the average of the two signals at 1.22 and 1.315  $\mu\text{m}$ , Fig. 4(a) implies essentially no detectable singlet oxygen signal. In contrast, Fig. 4(b) shows similar data, but after injection with ALA and after 50J of PDT treatment. The signal at 1.27  $\mu\text{m}$  is clearly larger than at the other two, off-band wavelengths and persists for a longer time.

During the PDT treatments, the optical fiber probe of the singlet oxygen monitor was moved to allow unimpeded access of the tumor by the cw treatment laser beam that covered the entire area of the tumor site ( $\sim 1$  cm diam). Subsequent to the delivery of a selected treatment fluence, the cw laser was shut off, and the fiber probe of the singlet oxygen monitor was

repositioned  $\sim 1.5$  mm from the tumor site. The diameter of the monitor diode laser beam on the tumor site was  $\sim 2$  to 3 mm. This removal and repositioning of the monitor beam before and after a treatment caused variations in the observed signal levels, presumably due to nonuniformities in the optical properties of the tissue (including the skin) of the subject animal. However, we measure the difference between the average of the two, out-of-band (with respect to singlet oxygen) emissions at 1.22 and 1.315  $\mu\text{m}$  and the in-band signal at 1.27  $\mu\text{m}$  to determine the relative singlet oxygen concentration. This variation is clearly shown in Figs. 4(a) and 4(b). In Fig. 4(a) (no PS), we observed signals at all three wavelengths that were nearly identical and larger than those of Fig. 4(b) (with PS). However, the signal detected at 1.27  $\mu\text{m}$  is larger than the signals at 1.22 and 1.315  $\mu\text{m}$  in Fig. 4(b). This is consistent with the production of singlet oxygen in the tumor.

The singlet oxygen signal was monitored in each animal, and Figs. 4(c) and 4(d) show the singlet oxygen production (the measured counts at 1.27  $\mu\text{m}$  minus the counts averaged at 1.22 and 1.315  $\mu\text{m}$ ) for two rats as a function of PDT light dosage. The data shown in Fig. 4(d) indicate a negative value for the singlet oxygen concentration for the no ALA case. This is a result of the background subtraction routine described before and represents the systematic uncertainty for the weak signals observed in the absence of a PS. The singlet oxygen signal was clearly higher after the initial PDT treatment. This may be due to increased oxygenation or blood flow to the

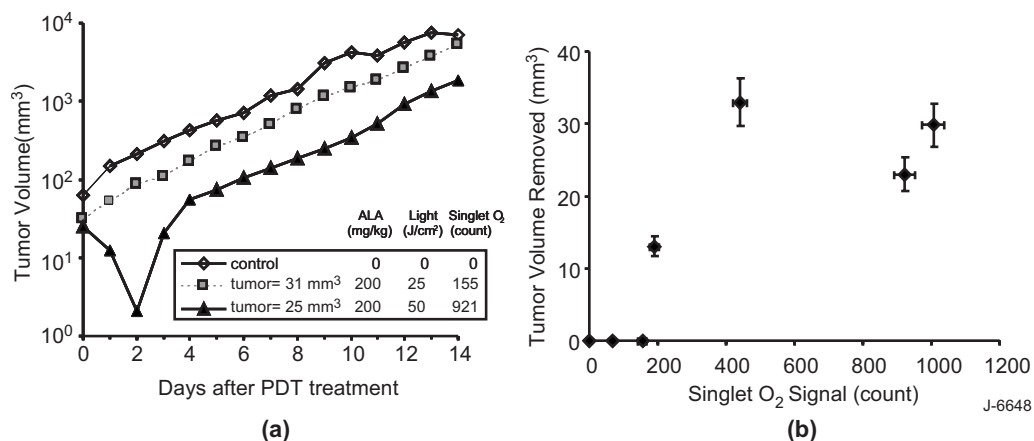


**Fig. 5** Tumor regression data: (a) three rats including one control, and (b) measured tumor regression as a function of singlet oxygen counts for a cohort of seven rats. Singlet oxygen counts are the cumulative values for the particular PDT treatment.

treated area. Indeed, several groups have reported enhanced blood flow and increased ground state oxygenation early in the PDT treatment process.<sup>13,14</sup> Cottrell et al. have also recently observed a formation of a photoproduct during ALA photobleaching, and the photoproduct is a PDT active species producing singlet oxygen.<sup>22</sup> They reported that this process increased the concentration of the photoproduct until about 15 J/cm<sup>2</sup> of fluence had been delivered. Note that some researchers<sup>23,24</sup> have attempted to develop PDT dosimeters based on the fluorescence intensity of the PS in the tumor, but photobleaching of the PS precludes this as an accurate method. The singlet oxygen production depends on all the parameters that affect PDT treatment: [PS], light dosage, and [O<sub>2</sub>].

### 3.3 Tumor Regression Study

Following the PDT treatment with different ALA dosages and light dosages, the tumor size was measured each day for 14 days. In Fig. 5, we present results of tumor growth and regression following the treatment. Figure 5(a) illustrates the tumor regression measured for three rats as a function of the singlet oxygen measured during the PDT treatment. One was in a control group that had no PDT treatment light or ALA. One rat produced a relatively small singlet oxygen signal of 155 counts and showed steady tumor growth similar to the control. The rat that produced the most singlet oxygen of 921 counts (approximately six times that of the one with 155 counts singlet oxygen) showed a tumor regression of ~90% two days after the treatment. Tumor growth then began again. The treatments were not intended to be curative.

In Fig. 5(b), we plot the tumor regression as a function of the singlet oxygen measured during the PDT light treatment in a group of seven rats. This plot shows a positive correlation between singlet oxygen production and tumor volume regression. The error bars represent the estimated statistical uncertainties in measuring tumor size and the standard deviations of the number of singlet oxygen photoelectrons detected. The data indicate larger systematic uncertainties in singlet oxygen production and tumor regression for different animals. Even with the rather large uncertainties and our very limited study, we observed a clear trend of larger tumor volume removal

with more singlet oxygen production during PDT light treatment. While these are preliminary data from a limited number of animals, there does appear to be a positive correlation of the volume of tumor regression and the amount of singlet oxygen produced. An extensive animal study is planned to further investigate this relationship with the goal of developing a statistically significant database.

## 4 Summary

We described a novel, fiber-coupled, diode laser-based system for measuring the production of singlet oxygen during PDT, and successfully applied this device to measure PDT produced singlet oxygen *in vivo*. Using tumor-laden rats, we observed singlet oxygen produced by PDT treatments with both *Cl-e6* and ALA. We also observed tumor regression that correlates with the measured singlet oxygen produced. Although these initial results display only moderate signal-to-noise ratios, there is a clear relationship between singlet oxygen production and tumor regression. This could potentially provide the critical parameter in PDT dosimetry and facilitate individual therapeutic design. We plan to enhance the sensitivity of the monitor and will complete a much more extensive animal study to further test the capability of monitoring singlet oxygen *in vivo*.

### Acknowledgments

This work was supported under a grant from the National Cancer Institute of the National Institutes of Health (grant number 5 R44 CA096243-03). We are grateful for this support. The authors would like to thank B. W. Pogue (Dartmouth College) and B. C. Wilson (University of Toronto, Canada) for helpful discussions.

### References

1. D. Phillips, "Photodynamic therapy," *Sci. Prog.* **77**, 295–316 (1994).
2. J. S. Dysart and M. S. Patterson, "Characterization of photofrin photobleaching for singlet oxygen dose estimation during photodynamic therapy of MLL cells *in vitro*," *Phys. Med. Biol.* **50**, 2597–2616 (2005).
3. M. Ochsner, "Photophysical and photobiological processes in the photodynamic therapy of tumors," *J. Photochem. Photobiol., B* **39**, 1–18 (1997).

4. K. R. Weishaupt, C. J. Gomer, and T. J. Dougherty, "Identification of singlet oxygen as the cytotoxic agent in photo-inactivation of a murine tumor," *Cancer Res.* **36**, 2326–2329 (1976).
5. D. Kessel and Y. Luo, "Mitochondrial photodamage and PDT-induced apoptosis," *J. Photochem. Photobiol., B* **4**, 89–95 (1998).
6. V. H. Fingar, T. J. Wieman, S. A. Wiehle, and P. B. Cerrito, "The role of microvascular damage in photodynamic therapy. The effect of treatment on vessel constriction, permeability, and leukocyte adhesion," *Cancer Res.* **52**, 4914–4921 (1992).
7. H. J. Laubach, S. K. Chang, S. Lee, I. Rizvi, D. Zurakowski, S. J. Davis, C. R. Taylor, and T. Hasan, "In vivo singlet oxygen dosimetry of clinical 5-aminolevulinic acid photodynamic therapy," *J. Biomed. Opt.* **13**, 050504 (2008).
8. B. C. Wilson, M. S. Patterson, and L. Lilge, "Implicit and explicit dosimetry in photodynamic therapy: a new paradigm," *Lasers Med. Sci.* **12**, 182–199 (1997).
9. M. J. Niedre, M. S. Patterson, and B. C. Wilson, "Direct near-infrared luminescence detection of singlet oxygen generated by photodynamic therapy in cells in vitro and tissues in vivo," *Photochem. Photobiol.* **75**, 382–391 (2002).
10. M. J. Niedre, C. S. Yu, M. S. Patterson, and B. C. Wilson, "Singlet oxygen luminescence as an in vivo photodynamic therapy dose metric: validation in normal mouse skin with topical amino-levulinic acid," *Br. J. Cancer* **92**, 298–304 (2005).
11. B. W. Pogue, R. D. Braun, J. L. Lanzen, C. Erikson, and M. W. Dewhirst, "Analysis of the heterogeneity of pO<sub>2</sub> dynamics during photodynamic therapy with verteporfin," *Photochem. Photobiol.* **74**, 700–706 (2001).
12. B. W. Henderson, T. M. Busch, L. A. Vaughan, N. P. Frawley, D. Babich, T. A. Sosa, J. D. Zollo, A. S. Dee, M. T. Cooper, D. A. Bellnier, W. R. Greco, and A. R. Oseroff, "Photofrin photodynamic therapy can significantly deplete or preserve oxygenation in human basal cell carcinomas during treatment, depending on fluence rate," *Cancer Res.* **60**, 525–529 (2000).
13. H. W. Wang, M. E. Putt, M. J. Emanuele, D. B. Shin, E. Glatstein, A. G. Yodh, and T. M. Busch, "Treatment-induced changes in tumor oxygenation predict photodynamic therapy outcome," *Cancer Res.* **64**, 7553–7561 (2004).
14. Q. Chen, Z. Huang, H. Chen, H. Shapiro, J. Beckers, and F. W. Hetzel, "Improvement of tumor response by manipulation of tumor oxygenation during photodynamic therapy," *Photochem. Photobiol.* **76**, 197–203 (2002).
15. S. J. Davis, L. Zhu, A. M. Minhaj, M. F. Hinds, S. Lee, P. B. Keating, D. I. Rosen, and T. Hasan, "Ultra-sensitive, diode laser-based monitor for singlet oxygen," *Proc. SPIE* **4952**, 140–148 (2003).
16. S. Lee, L. Zhu, A. Minhaj, M. F. Hinds, A. A. Ferrante, D. H. Vu, D. I. Rosen, S. J. Davis, and T. Hasan, "Diode laser monitor for singlet molecular oxygen," *Proc. SPIE* **5689**, 90–96 (2005).
17. S. Lee, L. Zhu, A. M. Minhaj, M. F. Hinds, D. H. Vu, D. I. Rosen, S. J. Davis, and T. Hasan, "Pulsed diode laser-based monitor for singlet molecular oxygen," *J. Biomed. Opt.* **13**, 034010 (2008).
18. T. Maisch, J. Baier, B. Franz, M. Maier, M. Landthaler, R. M. Szeimies, and W. Bäuml, "The role of singlet oxygen and oxygen concentration in photodynamic inactivation of bacteria," *Proc. Natl. Acad. Sci. U.S.A.* **104**, 7223–7228 (2007).
19. J. Yamamoto, S. Yamamoto, T. Hirano, S. Li, M. Koide, E. Kohno, M. Okada, C. Inenaga, T. Tokuyama, N. Yokota, S. Terakawa, and H. Namba, "Monitoring of singlet oxygen is useful for predicting the photodynamic effects in the treatment for experimental Glioma," *Clin. Cancer Res.* **12**, 7132–7139 (2006).
20. N. Solban, S. K. Pal, S. K. Alok, C. K. Sung, and T. Hasan, "Mechanistic investigation and implications of photodynamic therapy induction of vascular endothelial growth factor in prostate cancer," *Cancer Res.* **66**, 5633–5640 (2006).
21. B. Kosharsky, N. Solban, S. K. Chang, I. Rizvi, Y. Chang, and T. Hasan, "A mechanism-based combination therapy reduces local tumor growth and metastasis in an orthotopic model of prostate cancer," *Cancer Res.* **66**, 10953–10958 (2006).
22. W. J. Cottrell, A. D. Paquette, K. R. Keymel, T. H. Foster, and A. R. Oseroff, "Irradiance-dependent photobleaching and pain in delta-aminolevulinic acid-photodynamic therapy of superficial basal cell carcinomas," *Clin. Cancer Res.* **14**, 4475–4483 (2008).
23. I. A. Boere, D. J. Robinson, H. S. de Bruijn, J. van den Boogert, H. W. Tilanus, H. J. C. M. Sterenborg, and R. W. de Bruin, "Monitoring in situ dosimetry and protoporphyrin IX fluorescence photobleaching in the normal rat esophagus during 5-aminolevulinic acid photodynamic therapy," *Photochem. Photobiol.* **78**, 271–277 (2003).
24. T. J. Farrell, R. P. Hawkes, M. S. Patterson, and B. C. Wilson, "Modeling of Photosensitizer fluorescence emission and photobleaching for photodynamic therapy dosimetry," *Appl. Opt.* **37**, 7168–7183 (1998).